

THE NUZZ: NUMERICAL ZIGZAG SAMPLING FOR GENERAL MODELS

Simon Cotter*

Thomas House*

Filippo Pagani*†

March 10, 2020

Abstract

Markov chain Monte Carlo (MCMC) is a key algorithm in computational statistics, allowing for a large amount of versatility in both model and data. However, as datasets grow larger and models grow more complex, many popular MCMC algorithms become too computationally expensive to be practical. Recent progress has been made on this problem through development of MCMC algorithms based on Piecewise Deterministic Markov Processes (PDMPs). In particular, one variant the ZigZag process (a PDMP) has been shown to have the remarkable property of super-efficiency, meaning that the computational effort required to draw a sample from the posterior distribution in Bayesian inference need not grow with the size of the dataset. While there has understandably been a surge of theoretical studies following these results, PDMPs have so far only been implemented for models where certain gradients can be globally bounded to allow for simulation via thinning. This is not possible in many statistical contexts, and in others, even where a bound is available, it introduces inefficiencies that negate the effects of super-efficiency. Here, we present the Numerical ZigZag (NuZZ) algorithm, which is applicable to general statistical models, without the need for bounds on the gradient of the log posterior. This allows us to investigate: (i) how the ZigZag process behaves on some test problems with common challenging features; (ii) the performance of NuZZ compared to other numerical approaches to the ZigZag; (iii) the error between the target and sampled distributions as a function of computational effort for different MCMC algorithms including the NuZZ. Through a series of test problems we compare the mixing of the ZigZag process against other common methods. We present numerical evidence and an analytical argument that the Wasserstein distance between the target distribution and the invariant distribution of the NuZZ process is expected to exhibit asymptotically linearly dependence on the tolerances of both the numerical integration and root finding schemes used. Notably we present a real-life example which demonstrates that NuZZ can outperform not only the super-efficient version of the ZigZag process with thinning, but also well-established methods such as Hamiltonian Monte Carlo.

1 Introduction

1.1 Background

Markov Chain Monte Carlo (MCMC) methods are a mainstay of modern statistics [Brooks et al., 2011], and are employed in a wide variety of applications, such as astrophysics [The Dark Energy Survey Collaboration et al., 2017], epidemiology [House et al., 2016], chemistry [Cotter et al., 2019a, Cotter et al., 2019b] and finance [Kim et al., 1998]. The challenges that MCMC algorithms have to overcome nowadays are diverse, including multimodality of the posterior, complex non-linear dependencies between parameters, large number of parameters (sometimes called the ‘big- p ’ or ‘big- d ’ problem) [Cotter et al., 2013], and a large number of observations (sometimes called the ‘big- n ’ problem) [Bardenet et al., 2017].

*Department of Mathematics, The University of Manchester, Manchester, M13 9PL, UK.

†Corresponding Author: filippo.pagani@manchester.ac.uk

Common MCMC methods such as the Random Walk Metropolis (RWM) algorithm [Metropolis et al., 1953] offer simplicity and flexibility, but also have several limitations. Throughout the history of MCMC [Robert and Casella, 2011] there have been many attempts to improve algorithmic efficiency, including the work of [Hastings, 1970] in generalising the RWM approach, and the use of gradient information to explore the state space according to a discretised Langevin diffusion in the Metropolis-Adjusted Langevin Algorithm (MALA) [Roberts and Rosenthal, 1997]. Both of these methods rely on reversible dynamics that satisfies a detailed balance condition, used to ensure convergence to the appropriate limiting distribution.

Lifting the process simulated to a larger state space can aid exploration of the original state space, with one of the most successful such approaches being the Hamiltonian Monte Carlo (HMC) algorithm [Duane et al., 1987], and its equivalent on Riemannian manifolds (RMHMC) [Girolami et al., 2011]. HMC is obtained by adding momentum variables to the state space, while maintaining detailed balance and reversibility.

Recently, there has been investigation of the advantages of abandoning reversibility in favour of irreversible dynamics. This was initially carried out for discrete state spaces [Diaconis et al., 2000], with a more general method to construct these algorithms found in [Turitsyn et al., 2011], where a reversible process is ‘lifted’ to an enlarged state space that allows for more efficient exploration. In [Ma et al., 2016] the authors attempt to develop a framework for creating irreversible algorithms. In [Ottobre, 2016] the author considers the potential benefits of using irreversible diffusions as opposed to reversible ones.

In the physics literature, [Rapaport, 2009] and [Peters and de With, 2012] laid the foundation for the Bouncy Particle Sampler (BPS) [Bouchard-Côte et al., 2017], which abandons diffusions in favour of a completely irreversible, piecewise deterministic dynamics based on the theory developed in [Davis, 1984, Davis, 1993]. The link between the BPS and HMC is explored in [Deligiannidis et al., 2018].

Studying irreversible algorithms [Bierkens, 2015], Bierkens and Roberts [Bierkens and Roberts, 2016] discovered the Zig-Zag (ZZ) process, which is a variant of the Telegraph process [Kolesnik and Ratanov, 2013], a Piecewise Deterministic Markov Processes (PDMP) that is part of the same family as the BPS. The authors explored its statistical properties in [Bierkens and Duncan, 2016, Bierkens et al., 2016] for the purpose of sampling. The ZZ sampler [Bierkens and Roberts, 2016] is particularly appealing as when properly modified with global bounds for the switching rate, it has a computational cost per iteration that need not grow with the size of the data. This feature makes it particularly well suited for ‘tall, thin’ data, particularly multivariate datasets with a large number of observations, n , and a relatively small number of parameters, d , and thereby directly addresses the ‘big- n ’ problem.

The BPS sampler and the ZZ sampler are closely related, as they are both PDMPs that change direction at random times according to the arrival times of a Poisson process whose rate depends on the gradient of the target density. The main difference between them is the way the new direction is chosen. Moreover, they completely coincide when the state space has only one dimension. Conditions for ergodicity have been established for both algorithms [Bierkens et al., 2019, Durmus et al., 2019], and the Generalised Bouncy Particle Sampler [Wu and Robert, 2017] partially bridges the gap between the two.

Given their asymptotic efficiency, there has been a wealth of theoretical analysis of PDMPs in MCMC developed in recent years, e.g. [Bierkens et al., 2018, Zhao and Bouchard-Côte, 2019, Andrieu et al., 2019, Bierkens and Verduyn Lunel, 2019]. In [Vanetti et al., 2018], the authors provide insights into a general framework for construction of continuous and discrete time algorithms based on piecewise deterministic processes, and discuss some improvements that ameliorate some of the current challenges

that PDMP samplers face. There remains, however, a lack of guidance about which classes of statistical problems are well suited to the use of PDMP algorithms, and how those algorithms are best to be implemented. We will illustrate this lack of knowledge with an example.

1.2 Motivating example: Bayesian linear regression

The ZigZag sampler with control variates (ZZCV) algorithm has been shown to have a theoretical cost of $\mathcal{O}(1)$ in the number of observations n in the large data limit, $n \rightarrow \infty$ [Bierkens and Roberts, 2016]. For a given n , however, the cost of the algorithm will also be determined by other considerations such as the dimensionality of the problem, and sharpness of the bound on the gradient of the potential (a quantity proportional to the log density function, which we define precisely below). We provide here an example that demonstrates how the ZZCV method becomes significantly less efficient than the ZigZag sampler with inverse cdf using the full dataset, as the dimensionality of the problem is increased.

Consider a Bayesian linear regression model, $\mathbf{y} = \mathbf{X}\boldsymbol{\beta} + \boldsymbol{\varepsilon}$. We are interested in finding the posterior distribution over the length- d parameter vector $\boldsymbol{\beta}$, given the $n \times d$ matrix of independent variables \mathbf{X} , and the length- n vector of dependent variables, \mathbf{y} . The errors in the length- n vector $\boldsymbol{\varepsilon}$ are taken to be normally distributed, $\boldsymbol{\varepsilon} \sim \mathcal{N}(\mathbf{0}, \sigma^2 \mathbf{I})$, where $\mathbf{0}$ is a length- n vector with all zero elements and \mathbf{I} is the $n \times n$ identity matrix. Taking the prior on $\boldsymbol{\beta}$ to be improper, i.e. $\pi_0(\boldsymbol{\beta}) \propto 1$, the marginal posterior on the parameter vector given the observed data and standard deviation of the error has the simple form $\boldsymbol{\beta}|\{X, \mathbf{y}, \sigma\} \sim \mathcal{N}(\hat{\boldsymbol{\beta}}, \sigma^2(\mathbf{X}^\top \mathbf{X})^{-1})$, where we use hats to denote maximum-likelihood estimates (MLEs).

We apply this linear regression model to the House Prices dataset from [Kaggle, 2017]. The dataset is composed of $n = 1459$ house sales prices, along with $d = 80$ variables for each house, describing features such as position, type of heating, and type of bath. We selected this dataset because it has a reasonably high number of variables, many of which are categorical, as is often the case in real datasets. Missing values in the data were dealt with as suggested in [Gaudreau, 2017], and we coded categorical variables using dummy variables. We discarded the variables *Utilities* (type of utilities available), *TotalBsmntSF* (total square feet of basement area), and *GrLivArea* (above grade (ground) living area square feet), to avoid singularities in the matrix $(\mathbf{X}^\top \mathbf{X})^{-1}$, and the variable *Id* (identity number), which is not part of the analysis. Finally, we make the standard choice to use the logarithm of the sales price as the variable \mathbf{y} . This processing left us with $d = 77$ variables.

To simplify running the ZZCV algorithm, we do not estimate the error variance parameter σ^2 as part of the MCMC algorithm. Rather, we set it as exactly equal to its MLE, $\sigma = \hat{\sigma}$. We report a more detailed error analysis below, but for the purposes of motivating further algorithmic development, we define the efficiency of the ZZCV algorithm as the number of velocity switches per epoch (evaluation of the full likelihood function). When analytical solutions are available, it is possible to use the full dataset to have exactly one switch per epoch. In this framework, an algorithm that takes less than one epoch to produce one switch is regarded as more efficient than the baseline ZigZag sampler using analytical solutions and full data. We note again, however, that this is not a direct comparison, which will follow later, since the ZigZag and ZZCV are different processes, but is indicative of algorithmic efficiency.

We measured the efficiency of the ZZCV algorithm when run on the House Prices dataset for 100,000 switching points. The ratio of switching points to epochs was 2.32×10^{-3} , considerably less than the baseline value of one. We speculate that this is due to the presence of categorical variables, and to

a small value of $\hat{\sigma}^2 \approx 3 \times 10^{-4}$, resulting in particularly inefficient exploration of the target. We will revisit the results from this experiment in Section 5.2.7.

We replicated this loss of efficiency with a numerical experiment on simulated data. The synthetic dataset had fixed and known $\sigma^2 = 1.5$, a varying number of parameters d (from 2 to 80) and categorical regressors \mathbf{X} , represented by random integers from 0 to 4. The number of rows of the matrix \mathbf{X} was taken to be $n = 100$.

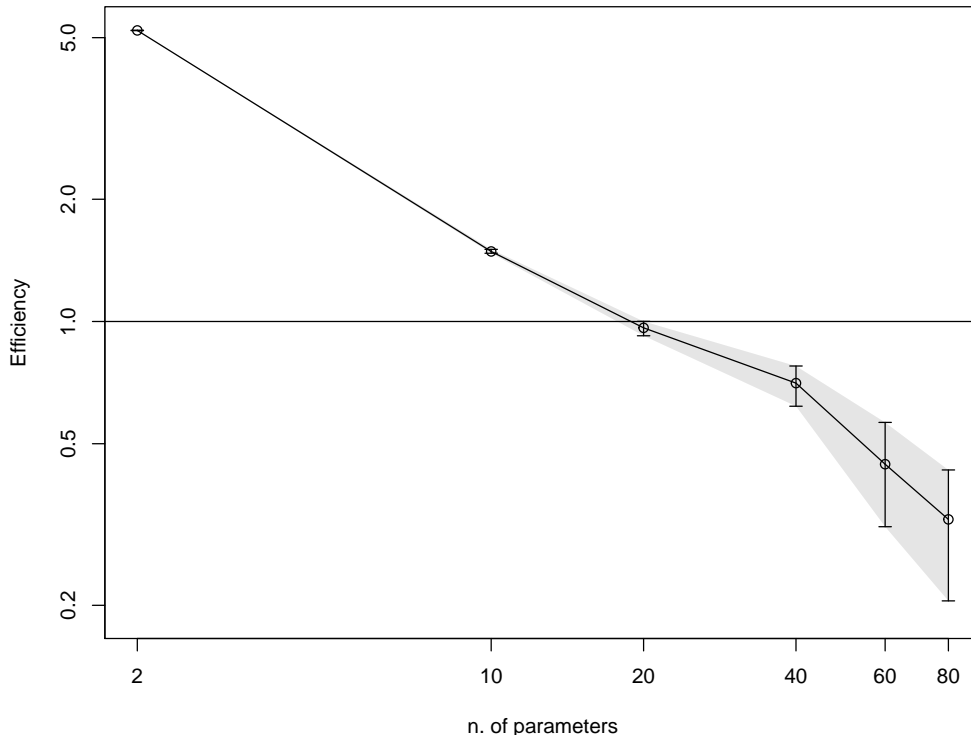


Figure 1: Efficiency of the ZZCV algorithm, defined as the number of velocity switches per epoch, for a set of synthetic linear regression problems, as a function of the dimension of the state space. The horizontal line at 1 represents the efficiency of the ZigZag sampler when analytical solutions are available.

Figure 1 shows the efficiency of the ZZCV algorithm, calculated as the number of velocity switches per epoch, as the number of model parameters grows. The shaded area represents the two sided 95% prediction interval, calculated on 40 runs for each dataset size. Although the reduction in performance of ZZCV while increasing d is not as severe as on the House Prices dataset, after around $d = 20$ parameters it is more efficient to use the whole dataset with a theoretical cost of $\mathcal{O}(n)$, rather than using exact subsampling for a theoretical cost of $\mathcal{O}(1)$.

Our results are, therefore, consistent with the considerations presented in [Bardenet et al., 2017]. While ZZ-based algorithms show great promise, their efficiency depends substantially on the data and model considered. Moreover, their applicability relies on analytic results which are only available for a small class of models.

1.3 Outline

In this work we aim to study the ZigZag dynamics and how well they explore distributions with specific features, often found in practical Bayesian statistics. In order to do this, we develop a numerical approximation to calculate the time to the next switch for general distributions, without requiring analytical solutions or bounds for the switching rate.

The paper is organised as follows. In Section 2 we review the technical details of the ZigZag process. In Section 3 we present an alternative algorithm, the Numerical ZigZag (NuZZ), which uses numerical methodology to compute switching times of the ZigZag process. In Section 4 we analyse the convergence of the invariant distribution of the NuZZ process as the numerical approximations used are refined. In Section 5 we present some numerical experiments which test the performance of a range of MCMC algorithms, including NuZZ and ZZCV, for a range of test problems with features often found in real-world models. Finally in Section 6 we conclude with some discussions of the results.

2 The ZigZag sampler

In this section we briefly overview the key components of the ZigZag process. The ZZ process is a PDMP [Davis, 1984] defined on $E = \mathcal{X} \times \mathcal{V} = \mathbb{R}^d \times \{+1, -1\}^d$. The process is described by two vectors in a d -dimensional space; its position \mathbf{x} , and its velocity \mathbf{v} . Between jumps, the ZZ process moves linearly and deterministically according to the ordinary differential equation

$$\frac{d\mathbf{x}}{dt} = \mathbf{v} \quad \Rightarrow \quad \mathbf{x}_{t+s} = \mathbf{x}_t + s\mathbf{v}, \quad (1)$$

with $t, s \in \mathbb{R}^+$, until after a waiting time of $\tau \in \mathbb{R}^+$, a velocity switch occurs, and one of the components of \mathbf{v} switches sign. The switching of the i -th component of the velocity is a one-step Poisson process with rate $\lambda_i(\mathbf{x}, \mathbf{v})$. This produces ‘zig-zag’ patterns such as those seen in Figure 2, motivating its name.

More explicitly, the ZigZag process has infinitesimal generator \mathcal{U}_{ZZ} given by

$$\mathcal{U}_{ZZ}f(\mathbf{x}, \mathbf{v}) = \sum_{i=1}^d \left\{ v_i \frac{\partial f}{\partial x_i} + \lambda_i(\mathbf{x}, \mathbf{v}) (f(\mathbf{x}, \mathbf{F}_i(\mathbf{v})) - f(\mathbf{x}, \mathbf{v})) \right\}, \quad (2)$$

where $f \in C(E)$, the space of continuous functions on the domain $E = \mathcal{X}^d \times \mathcal{V}^d$, and the vector-valued function $\mathbf{F}_i : \mathcal{V} \rightarrow \mathcal{V}$ represents the operation of changing the sign of the i -th component of the velocity, mapping the vector \mathbf{v} to an identical vector but with the i -th velocity’s sign reversed [Bierkens et al., 2016].

The process, as represented by the set of switching points, velocities and times, $\{\mathbf{X}_k, \mathbf{V}_k, T_k\}_{k=1}^K$, and the linear deterministic dynamics (1) in between, is strong Markov and exponentially ergodic [Bierkens et al., 2016, Bierkens et al., 2019]. The process has a unique stationary distribution that can be tuned by changing the switching rates $\lambda_i(\mathbf{x}, \mathbf{v})$.

Let the target distribution be in the form

$$\pi(\mathbf{x}) = \frac{1}{Z} e^{-U(\mathbf{x})},$$

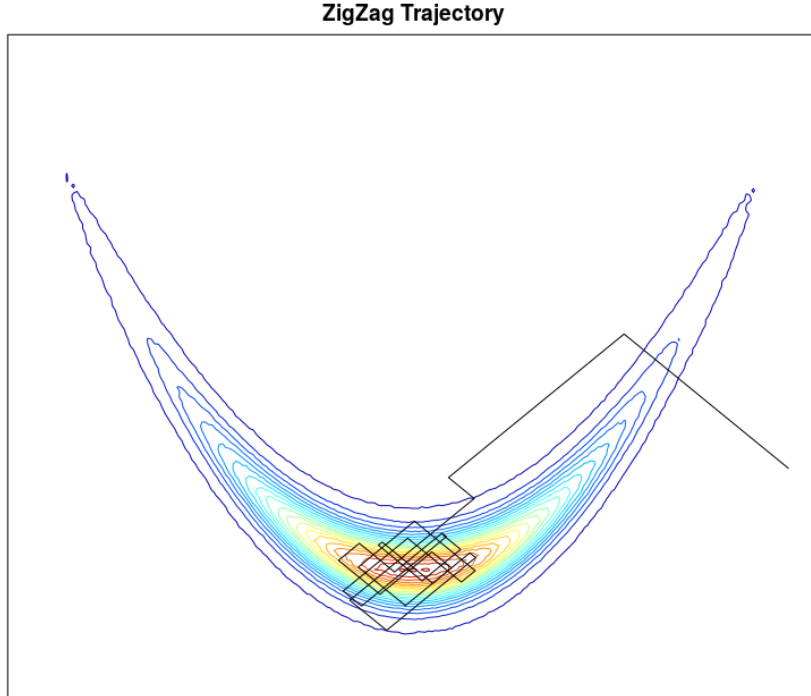


Figure 2: Example ZigZag trajectory. The target is a 2-dimensional Rosenbrock distribution.

where $U : \mathbb{R}^d \rightarrow \mathbb{R}$ is the potential, and Z is a normalising constant that is typically unknown. Let $\gamma_i(\mathbf{x}, \mathbf{v}) = \gamma_i(\mathbf{x}, \mathbf{F}_i(\mathbf{v}))$ be positive functions. Taking

$$\lambda_i(\mathbf{x}, \mathbf{v}) = \left(0 \vee v_i \frac{\partial U}{\partial x_i} \right) + \gamma_i(\mathbf{x}, \mathbf{v}) \quad (3)$$

guarantees that the process converges to the target distribution of interest, $\pi(\mathbf{x})$ [Bierkens et al., 2016].

2.1 Sampling the switching time

Switches in \mathbf{v} occur for each component i , and are distributed as the interarrival times of an inhomogeneous Poisson process with rate $\lambda_i(\mathbf{x}, \mathbf{v})$. If we therefore start at time $t = 0$, then the time τ_i to the next switch in the i -th component, conditional on no other switches happening, has distribution function

$$P(\tau_i) = 1 - \exp \left(- \int_0^{\tau_i} \lambda_i(\mathbf{x}(s), \mathbf{v}) ds \right). \quad (4)$$

When a switch event occurs in the i -th component of \mathbf{v} , the process switches velocity in that component, as denoted by the change of sign through the function $\mathbf{F}_i(\mathbf{v})$. A waiting time τ_i is sampled for each component with law given by (4), then the first switch occurs at time τ , with

$$\tau = \min_{i=1, \dots, d} \tau_i, \quad i^* := \arg \min_{i=1, \dots, d} \tau_i.$$

The evolution of the system after τ now follows a different trajectory, changing from $\mathbf{x}(0) + \mathbf{v}s$ to $\mathbf{x}(\tau) + \mathbf{F}_{i^*}(\mathbf{v})(s - \tau)$, meaning that all the larger $\{\tau_i\}_{i=1}^d$ with $i \neq i^*$ are discarded.

This method for sampling the switching times requires realisations of d random variables with densities given by (4), where d is the number of components of the ZigZag process, i.e. the number of parameters to be estimated via MCMC.

2.2 Poisson sampling via thinning

Sampling τ_i from equation (4) requires solving the integral in the exponential, which is often very difficult as the rates λ_i depend on the posterior in a complex way as shown in equation (3). Analytic solutions are rarely available and problem-dependent.

In [Bierkens et al., 2016] the authors propose the method of thinning to sample the waiting times to the next switch, τ_i . If the Jacobian or Hessian of the target $\pi(\mathbf{x})$ is bounded, then there exists a bound $\bar{\lambda}_i(\mathbf{x}, \mathbf{v}) \geq \lambda_i(\mathbf{x}, \mathbf{v})$, $\forall \mathbf{x}, \mathbf{v}, i$. The bound $\bar{\lambda}_i$ can be used instead of λ_i in equation (4), so that $p(\tau_i)$ becomes a simpler distribution. Once the τ_i are sampled and the time τ to the next switch is found, the proposed velocity switch occurs with probability $\lambda_{i^*}/\bar{\lambda}_{i^*}$, to account for the fact that τ was not sampled from the correct distribution. If the switch is rejected, there is no change in \mathbf{v} , the process moves linearly to $\mathbf{x} + \tau\mathbf{v}$, and new switching times are sampled.

Sampling the switching times via thinning extends the ZigZag sampler to a wider class of models than those where an analytic solution is available, and forms the basis for the ZZCV algorithm. However, implementations of this method can be very inefficient in practice, as shown in Figure 1.

3 Numerical ZigZag (NuZZ)

The ZigZag sampler described in Section 2 relies on the availability of an easy way to sample from Equation 4, or a bound for λ_i . In this section we extend the ZigZag algorithm to sample from arbitrary targets via numerical approximation of the switching times.

3.1 Numerical integration

In order to ameliorate the issues described in Section 1.2, it is possible to reformulate the problem of finding the time to the next velocity switch in a more convenient way. This approach is based on the Sellke construction [Sellke, 1983], and we note that picking τ_i with law (4) is equivalent to finding $\tau_i > 0$ such that

$$g(\tau_i) = \int_0^{\tau_i} \lambda_i(\mathbf{x}(s), \mathbf{v}) ds - Q = 0, \quad (5)$$

where $Q \sim \text{Exp}(1)$. Ergo, finding τ_i is equivalent to finding the root of the function $g(\tau_i)$, which can be accomplished numerically for a very wide class of models. There are, however, a number of problems to overcome. The function g is in $C^1(\mathbb{R}) \setminus C^2(\mathbb{R})$, and in practice it often increases very steeply when moving into the tails of the distribution. The numerical method used to solve the integral in (5) up to some $\hat{\tau}$ should be chosen on the basis of its efficient and accurate approximation of such a problem. The function g is differentiable but not analytic, therefore integrators like Runge-Kutta perform unreliably. In particular, the first derivative of λ_i is only piecewise continuous, which also creates problems for common root finding methods like Newton-Raphson.

The combination of methods we implemented was the QAGS (Quadrature Adaptive Gauss-Kronrod Singularities) integration routine from the GSL library [Galassi, M., 2017], combined with Brent's

method [Press et al., 2007] for finding the root. Brent’s method combines bisection (which does not rely on derivatives, but only converges linearly), inverse quadratic interpolation, bracketing of the root, and other techniques to perform quickly when the problem is relatively simple, and robustly when the problem is relatively hard, making it particularly suitable for the task in hand.

3.2 Efficient implementation

The ZigZag Sampler discussed in Section 2.1 relies on sampling a switching time τ_i for each component, then taking the minimum $\tau = \min_{i=1,\dots,d} \tau_i$. This approach requires sampling d random variables with densities (4) for each iteration. However, it is possible to reduce the cost to only one such sample per iteration, plus a draw from a multinomial distribution, by using the following procedure. First, Sample τ such that

$$\int_0^\tau \Lambda(\mathbf{x}(s), \mathbf{v}) ds = Q \sim \text{Exp}(1), \quad (6)$$

where $\Lambda(\mathbf{x}(s), \mathbf{v}) = \sum_{i=1}^d \lambda_i(\mathbf{x}(s), \mathbf{v})$ is the total rate of switching in any component. Then sample the index of the first component to switch, i^* , as a multinomial distribution with i -th cell probability $\lambda_i(\mathbf{x}(\tau), \mathbf{v})/\Lambda(\mathbf{x}(\tau), \mathbf{v})$. The last step can be achieved efficiently by taking i^* such that

$$i^* = \min \left\{ l \in \{1, \dots, d\} \mid \sum_{i=1}^l \frac{\lambda_i(\mathbf{x}(\tau), \mathbf{v})}{\Lambda(\mathbf{x}(\tau), \mathbf{v})} \geq U \right\}, \quad (7)$$

where $U \sim \text{Unif}(0, 1)$, and finding i^* by bisection search. This sampling method is used in the Gillespie algorithm, for Monte Carlo simulation of chemical reaction networks [Gillespie, 1977]. In our specific case, we can prove that the efficient implementation targets the correct invariant distribution by looking at the generator.

Proposition 1. *A ZigZag process where switches happen at rate $\Lambda(\mathbf{x}(s), \mathbf{v}) = \sum_{i=1}^d \lambda_i(\mathbf{x}(s), \mathbf{v})$, and the index of the velocity component to switch is distributed as*

$$i^* \sim \text{Multi} \left(\frac{\lambda_i(\mathbf{x}(\tau), \mathbf{v})}{\Lambda(\mathbf{x}(\tau), \mathbf{v})} \right), \quad (8)$$

targets the same invariant distribution $\pi(\mathbf{x})$ as the ZigZag process with generator given in (2).

Proof. Following [Davis, 1984, Davis, 1993], the generator of the process described above is

$$\mathcal{U}_\Lambda f(\mathbf{x}, \mathbf{v}) = \sum_{i=1}^d v_i \frac{\partial f}{\partial x_i} + \Lambda(\mathbf{x}, \mathbf{v}) \left(\sum_{r=1}^d \frac{\lambda_r(\mathbf{x}, \mathbf{v})}{\Lambda(\mathbf{x}, \mathbf{v})} (f(\mathbf{x}, \mathbf{F}_r(\mathbf{v})) - f(\mathbf{x}, \mathbf{v})) \right), \quad (9)$$

where the first term represents the drift and the second the velocity switch. The process switches velocities with overall rate Λ , whereby the index of the switching component r is sampled according to the multinomial transition kernel in (8). By carrying out some standard manipulations, Equation (9) reduces to

$$\mathcal{U}_\Lambda f(\mathbf{x}, \mathbf{v}) = \sum_{i=1}^d \left(v_i \frac{\partial f(\mathbf{x}, \mathbf{v})}{\partial x_i} + \lambda_i(\mathbf{x}, \mathbf{v}) (f(\mathbf{x}, \mathbf{F}_i(\mathbf{v})) - f(\mathbf{x}, \mathbf{v})) \right),$$

which is identical to Equation (2), i.e. the generator of the original ZigZag process, and therefore the two processes are equivalent. \square

Importantly, sampling τ in this way reduces the number of integrals to be computed numerically from d to 1, at the price of a slight increase in the complexity of the integrand. Moreover, there may be more efficient implementations than bisection to find i^* , which may reduce the computational complexity further.

Algorithm 1: Numerical ZigZag (NuZZ)

- 1 Initialise: $t = 0$; $\mathbf{x}(0) = \mathbf{x}_{\text{init}}$; $\mathbf{v}(0) = \mathbf{v}_{\text{init}}$; $N =$ number of desired switching points.
 - 2 **for** $k = 1 : N$ **do**
 - 3 Sample $Q \sim \text{Exp}(1)$
 - 4 Calculate τ such that $\int_0^\tau \Lambda(\mathbf{x}(s), \mathbf{v}) ds - Q = 0$
 - 5 Set $\mathbf{x}(t + \tau) = \mathbf{x}(t) + \tau \mathbf{v}(t)$
 - 6 Sample $i^* \sim \text{Multi} \left(\frac{\lambda_i(\mathbf{x}(t+\tau), \mathbf{v}(t))}{\Lambda(\mathbf{x}(t+\tau), \mathbf{v}(t))} \right)$
 - 7 Set $\mathbf{v}(t + \tau) = \mathbf{F}_{i^*}(\mathbf{v}(t))$
 - 8 Record switching point $\mathbf{X}_k = \mathbf{x}(t + \tau)$, $\mathbf{V}_k = \mathbf{v}(t + \tau)$, $T_k = t + \tau$.
-

It is worth pointing out that the benefits of this implementation of the ZigZag Sampler, i.e. working with the sum of rates, are not only applicable to the NuZZ algorithm. The approach can be applied to other ZigZag-based algorithms and PDMPs, and in fact it synergises particularly well with the ZigZag algorithm with control variates. In the case of a ZZCV algorithm on a Logit model, the bound $\bar{\lambda}_i$ is linear, i.e. $\bar{\lambda}_i(\mathbf{x}(s), \mathbf{v}) = a_i(\mathbf{x}, \mathbf{v}) + s b_i(\mathbf{x}, \mathbf{v})$. Equation (6) can be rewritten as

$$\int_0^\tau \sum_{i=1}^d (a_i + s b_i) ds = \int_0^\tau (A + sB) ds = Q, \quad (10)$$

where $A = \sum_{i=1}^d a_i$ and $B = \sum_{i=1}^d b_i$. Equation (10) can then be solved analytically, and i^* can be sampled from a multinomial with cell probability $\bar{\lambda}_i(\mathbf{x}(\tau), \mathbf{v})/\Lambda(\mathbf{x}(\tau), \mathbf{v}) = (a_i + \tau b_i)/(A + \tau B)$. Finally, the proposed τ is accepted as a switching time with probability $\lambda_i(\mathbf{x}(\tau), \mathbf{v})/\bar{\lambda}_i(\mathbf{x}(\tau), \mathbf{v})$, otherwise the dynamics moves on to $\mathbf{x} + \tau \mathbf{v}$, \mathbf{v} is unchanged, and a new potential switching time is sampled.

3.3 Formal analysis as a PDMP

While one can view NuZZ as simply a way to simulate the ZigZag process, it is also possible to define it as a PDMP in its own right. We call this Markov process the Sellke ZigZag (SeZZ) due to its origin in the Sellke Construction [Sellke, 1983]. We present this analysis first, to give confidence that the Sellke construction is correct in this specific context. Secondly we do so because the method of analysis may be applicable to other PDMPs used in MCMC. Lastly it will allow us to improve our understanding of the propagation of numerical errors in the algorithm.

For simplicity, we will work in the one-dimensional ($d = 1$) case, although it is possible to extend the analysis to d dimensions by indexing relevant quantities with $i = 1, \dots, d$ and summing over i , similarly to [Bierkens et al., 2016].

We start with Equation (6), and define a discrepancy variable $q(t)$ such that

$$q(t) = Q - \int_0^t \Lambda(x(s), v) ds, \quad t \in [0, \tau]. \quad (11)$$

Using Leibniz's rule, Equation (11) can be differentiated with respect to time to recast the integral Equation (6) as a boundary value problem for a differential equation with random initial condition,

namely

$$\frac{dq}{dt} = -\Lambda(x(t), v), \quad q(0) = Q \sim \text{Exp}(1), \quad q(\tau) = 0. \quad (12)$$

Between switches, and provided $q(t) > 0$, the dynamics of q are determined by this differential equation, as does the differential equation (1) for the dynamics of the state x . We can therefore add the discrepancy variable $q(t)$ to the existing position and velocity variables, $x(t)$ and $v(t)$. The variable q is defined on the space $\mathcal{Q} = [0, \infty)$, which decomposes into $\mathcal{Q}_0 = (0, \infty)$ and $\{0\}$. Following [Davis, 1993], we let $E = \mathcal{X} \times \mathcal{V} \times \mathcal{Q}_0$ be the interior of the state space, and $\Gamma = \mathcal{X} \times \mathcal{V} \times \{0\}$ be an active boundary of the state space. Note that $\mathcal{X} = \mathbb{R}$ and $\mathcal{V} = \{-1, +1\}$. In E , there are no switches and so the process is generated by the drift operator

$$\mathcal{D}f(x, v, q) = v \frac{\partial f}{\partial x} - \Lambda(x, v) \frac{\partial f}{\partial q}. \quad (13)$$

Eventually the function $q(t)$ reaches zero, causing the velocity to switch. This corresponds to contact with the active boundary Γ , at which point the sign of v is flipped and q is refreshed with a new exponential random variable. This is expressed through the boundary operator

$$\mathcal{C}f(x, v, 0) = \int_{\mathcal{Q}_0} e^{-q} f(x, v, q) dq - f(x, v, 0). \quad (14)$$

Between them, (13) and (14) define the *extended generator* of the SeZZ process, which forms the basis for its analysis.

Theorem 2. *The one-dimensional SeZZ process with extended generator given by (13) and (14) targets the marginal stationary distribution $\pi(x)$.*

Proof. Following [Davis, 1993], SeZZ targets the stationary measure $\mu(dx \times dv \times dq) = \pi(x, v, q) dx dv dq$ if

$$\int_E \mathcal{D}f(x, v, q) \mu(dx \times dv \times dq) + \int_{\Gamma} \mathcal{C}f(x, v, 0) \rho(dx \times dv) = 0, \quad (15)$$

where the measure ρ is induced on the boundary by μ and the process. Following [Löpker and Palmowski, 2013], this is equal to

$$\rho(dx \times dv) = \Lambda(x, v) \pi(x, v, 0) dx dv.$$

To demonstrate the desired result, it will be sufficient to show that Equation (15) is satisfied for

$$\pi(x, v, q) = \frac{1}{Z} e^{-U(x)} \times \frac{1}{2} \times e^{-q},$$

with no atoms at infinity. Substituting into Equation (15) above gives

$$\begin{aligned} \int_{\mathcal{X}} \sum_{v \in \mathcal{V}} \int_{\mathcal{Q}_0} \left(v \frac{\partial f}{\partial x} \Big|_{(x, v, q)} - \Lambda(x, v) \frac{\partial f}{\partial q} \Big|_{(x, v, q)} \right) e^{-U(x)-q} dq dx \\ + \int_{\mathcal{X}} \sum_{v \in \mathcal{V}} \left(\int_{\mathcal{Q}_0} f(x, -v, q) e^{-q} dq - f(x, v, 0) \right) \Lambda(x, v) e^{-U(x)} dx = 0, \end{aligned} \quad (16)$$

where the common constant $1/2Z$ has been cancelled. This equality follows by integration by parts and rearranging terms as shown in Appendix A. \square

We will study the behaviour of the NuZZ process i.e. the SeZZ process with numerical error in the next section.

4 Error analysis

4.1 Numerical error

In Section 3.1 we described how NuZZ relies on two different numerical methods to function: an integrator and a root-finding method. Let ε_{int} be the error tolerance set for the integration routine, and let ε_{Bre} be the tolerance level specified for Brent's root finding algorithm. The error at the final iteration of root finding algorithm can be written as

$$\eta_{\text{Bre}} = \int_0^{\tilde{\tau}} \tilde{\Lambda}(s) ds - Q, \quad Q \sim \text{Exp}(1), \quad (17)$$

where $\tilde{\Lambda}$ is the piecewise polynomial approximation to Λ used in the integration routine, and $\tilde{\tau} \neq \tau$ is the final root returned by the algorithm. Adding and subtracting terms to equation (17), and substituting in equation (6), we obtain

$$\eta_{\text{Bre}} = \underbrace{\int_0^{\tilde{\tau}} \tilde{\Lambda}(s) ds - \int_0^{\tilde{\tau}} \Lambda(s) ds}_{\eta_{\text{int}}} + \underbrace{\int_0^{\tilde{\tau}} \Lambda(s) ds - \int_0^{\tau} \Lambda(s) ds}_{\eta_{\text{root}}},$$

where η_{int} represents the error in the numerical integration routine, while η_{root} represents the error in the root finding routine, if the integrals were calculated exactly and on the correct rate.

Brent's method stops iterating when $|\eta_{\text{Bre}}| \leq \varepsilon_{\text{Bre}}$, so the root finding error would be

$$|\eta_{\text{root}}| = |\eta_{\text{Bre}} - \eta_{\text{int}}| \leq \varepsilon_{\text{Bre}} + \varepsilon_{\text{int}}.$$

This means that the algorithm targets a perturbation of the posterior, but as $\varepsilon_{\text{Bre}}, \varepsilon_{\text{int}} \rightarrow 0$, then $\varepsilon_{\text{root}} \rightarrow 0$, and therefore one would hope the sample provided by the algorithm is from the exact stationary measure. We argue that this heuristic holds in Section 4.2.

In our specific case, the integration routine is adaptive, and it stops improving the result when the size of η_{int} , the estimated error given the current number of nodes, is below the tolerance threshold ε_{int} .

4.2 Convergence with numerical error

In Section 3.3 we studied the behaviour of the NuZZ algorithm in complete absence of numerical errors. In this section we study how NuZZ converges to the true posterior as the numerical errors approach zero. In order to do that, let us write equation (15) for a 1- d NuZZ algorithm:

$$\int_E \tilde{\mathcal{D}}f(x, v, q) \tilde{\mu}(dx \times dv \times dq) + \int_{\Gamma} \tilde{\mathcal{C}}f(x, v, 0) \tilde{\rho}(dx \times dv) = 0, \quad (18)$$

where we use a tilde (i.e. $\tilde{}$) to denote terms that are perturbed by the sources of numerical error under consideration. In particular, the operator

$$\tilde{\mathcal{D}}f(x, v, q) = v \frac{\partial f}{\partial x} - \tilde{\Lambda}(x, v) \frac{\partial f}{\partial q} \quad (19)$$

encodes the fact that the error function $q(t)$ does not decrease according to the true rate Λ but instead according to its piecewise polynomial approximation $\tilde{\Lambda}$. Also, the operator

$$\tilde{\mathcal{C}}f(x, v, 0) = \int_{\mathcal{Q}_0} e^{-q+\eta_{\text{Bre}}(x,v,q)} f(x, -v, q) dq - f(x, v, 0) \quad (20)$$

represents switches in velocity as before. However, when a new $Q \sim \text{Exp}(1)$ is sampled, that value is shifted by a deterministic value η_{Bre} , which encodes the root-finding error as defined in Section 4.1 above. Both sources of numerical error will then perturb the invariant distributions so that

$$d\tilde{\mu} = \frac{1}{2Z} e^{-U(x)-q-\Delta(x,v,q)} dq dx, \quad d\tilde{\rho} = \tilde{\Lambda}(x, v, 0) \frac{1}{2Z} e^{-U(x)-q-\Delta(x,v,0)} dx.$$

The function Δ is therefore a placeholder for the perturbation to the invariant distribution due to numerical error. In practice, we are only interested in the desired measure on \mathcal{X} , $d\varphi \propto e^{-U(x)} dx$, as well as its numerically perturbed counterpart, $d\tilde{\varphi}$. Typically, the distance between two such measures will be quantified using an integral metric of the form

$$d_{\mathcal{H}}(\tilde{\varphi}, \varphi) = \sup_{h \in \mathcal{H}} \left| \int_{\mathcal{X}} h d\tilde{\varphi} - \int_{\mathcal{X}} h d\varphi \right|, \quad (21)$$

for some class of functions \mathcal{H} , with well-studied metrics in this class being the Wasserstein metric, the Total Variation metric, or the Kolmogorov metric [Ross, 2011]. Here, we define the operator \mathcal{A} such that

$$\begin{aligned} \mathcal{A}f(x, v, q) = \frac{1}{2} \sum_{\mathcal{V}} \left(\int_{\mathcal{Q}} \left(v \frac{\partial f}{\partial x} - \Lambda(x, v) \frac{\partial f}{\partial q} \right) e^{-q} dq \right. \\ \left. + \tilde{\Lambda}(x, v) \int_{\mathcal{Q}_0} f(x, -v, q) e^{-q} dq - \tilde{\Lambda}(x, v) f(x, v, 0) \right). \end{aligned} \quad (22)$$

Such an operator allows us to define the Stein discrepancy between $\tilde{\varphi}$ and φ as

$$d_{\mathcal{F}}(\tilde{\varphi}, \varphi) = \sup_{f \in \mathcal{F}} \left| \int \mathcal{A}f d\tilde{\varphi} - \int \mathcal{A}f d\varphi \right|, \quad (23)$$

for \mathcal{A} as in (22). Equation (23) is then a special case of (21) with $\mathcal{H} = \{\mathcal{A}f | f \in \mathcal{F}\}$, and \mathcal{F} is a subset of the class of functions of the form $f(x, v, q)$ which have a continuous first derivative in their first and third argument. Next, following a similar approach to [Huggins and Zou, 2017], define

$$\begin{aligned} \tilde{\mathcal{A}}f = \frac{1}{2} \sum_{\mathcal{V}} \left(\int_{\mathcal{Q}} \left(v \frac{\partial f}{\partial x} - \tilde{\Lambda}(x, v) \frac{\partial f}{\partial q} \right) e^{-q} dq \right. \\ \left. + \tilde{\Lambda}(x, v) \int_{\mathcal{Q}_0} f(x, -v, q) e^{-q+\eta_{\text{Bre}}(x,v,q)} dq - \tilde{\Lambda}(x, v) f(x, v, 0) \right). \end{aligned} \quad (24)$$

Note that Equations (15) and (18) together (22) and (24) give that both $E_{\varphi}[\mathcal{A}f] = 0$ and $E_{\tilde{\varphi}}[\tilde{\mathcal{A}}f] = 0$, which we can substitute into Equation (23) to give

$$\begin{aligned} d_{\mathcal{F}}(\tilde{\varphi}, \varphi) &= \sup_{f \in \mathcal{F}} \left| \int \mathcal{A}f d\tilde{\varphi} - \int \tilde{\mathcal{A}}f d\tilde{\varphi} \right| \\ &= \sup_{f \in \mathcal{F}} \left| \int_E \mathcal{D}f(x, v, q) d\tilde{\mu} + \int_{\Gamma} \mathcal{C}f(x, v, 0) d\tilde{\rho} - \int_E \tilde{\mathcal{D}}f(x, v, q) d\tilde{\mu} - \int_{\Gamma} \tilde{\mathcal{C}}f(x, v, 0) d\tilde{\rho} \right| \\ &= \sup_{f \in \mathcal{F}} \left| - \int_E (\Lambda(x, v) - \tilde{\Lambda}(x, v, q)) \frac{\partial f}{\partial q} d\tilde{\mu} + \int_{\Gamma} e^{-q} f(x, -v, q) (1 - e^{\eta_{\text{Bre}}(x,v,q)}) d\tilde{\rho} \right|. \end{aligned} \quad (25)$$

This equation links the discrepancy between measures to the numerical errors in the algorithm. We will now consider how this is expected to lead to bounds of the distance between measures in terms of numerical tolerances. The argument will be informal to avoid excessive technical detail.

First we note that with the appropriate assumptions on f , the function h can be taken to be 1-Lipschitz, which would imply that $d_{\mathcal{F}}$ is equal to the Wasserstein distance. Secondly, the difference between $\tilde{\Lambda}$ and Λ in the first term of the right-hand side of Equation (25) will generally be bounded by a constant κ_{int} multiplied by the integration tolerance ε_{int} . For example, in a Gauss-Kronrod integration scheme with m nodes, $\kappa_{\text{int}} = m$. Finally, we will assume that $\exp(\eta_{\text{Bre}}(x, v, q))$ is regular enough to admit a first order Taylor expansion. In turn, the Taylor expansion can be bounded from above substituting ε_{Bre} for η_{Bre} . Combining these assumptions with the results in Equation (25) we obtain

$$d_{\text{W}}(\tilde{\varphi}, \varphi) \leq \left| \kappa_{\text{int}} \int_E \frac{\partial f}{\partial q} d\tilde{\mu} \right| \varepsilon_{\text{int}} + \left| \kappa_{\text{Bre}} \int_{\Gamma} e^{-q} f(x, -v, q) d\tilde{\rho} \right| \varepsilon_{\text{Bre}} + \mathcal{O}(\varepsilon_{\text{Bre}}^2), \quad \forall f \in \mathcal{F}. \quad (26)$$

This demonstrates that we expect asymptotically linear errors in the numerical tolerances. In Section 5.1.3 we provide empirical evidence for the conclusions of this discussion.

5 Numerical experiments

We now study how the ZigZag process in various forms compares to other popular MCMC algorithms on test problems with features that are often found in practice. These features include high linear correlation, different length scales, high dimension, fat tails, and position-dependent correlation structure. We also return to the real House Price dataset from Section 1.2.

5.1 Methodology

5.1.1 Algorithm choice

In the following sections, we aim to compare the NuZZ method against three popular algorithms. In the figures that follow, the Random Walk Metropolis method is represented by the black \circ line labelled *RWM* in plots, Hamiltonian Monte Carlo by the green $+$ line labelled *HMC*, and the simplified Manifold MALA by the red \triangle line labelled *sMMALA* [Girolami et al., 2011].

For each example, we test two versions of NuZZ. The blue \times line labelled *NuZZepoch* represents the performance of the NuZZ algorithm when every epoch is counted. The current implementation of NuZZ is expensive in these terms, as for each root, $\Lambda(\mathbf{x}(s), \mathbf{v})$ (at the cost of one epoch) has to be evaluated for each root finding iteration, for each node of the numerical integral. Therefore the *NuZZepoch* line can be considered as a lower bound for the performance of the algorithm. However, the yellow line labelled *NuZZroot*, represents the performance of NuZZ when counting one epoch for each root only, which would be the performance of the algorithm if an analytical solution to equation (6) were available. The yellow line therefore represents an upper bound to the performance of NuZZ, and indeed any ZigZag Sampler. We run both algorithms with absolute tolerance of 10^{-10} for the integration routine, and 10^{-10} for Brent’s method.

For each model, we gave ourselves a computational budget of 6×10^6 epochs, and counted one epoch every time the full gradient or one likelihood evaluation is completed. For the sMMALA, we ignored the computational cost of computing the Hessian matrix, since depending on the problem, the actual cost of this will be highly variable.

The ZigZag-like algorithms that we study return a trajectory which is represented by a series of switching points. These trajectories then have to be uniformly subsampled to obtain an actual sample from the target distribution. In our experiments we obtained 8×10^6 samples.

Note that we are not able to implement the ZZCV for many of these examples for which good global bounds on the switching rates are (practically) impossible to obtain.

5.1.2 Performance evaluation

We chose as a measure of algorithm performance the largest Kolmogorov-Smirnov (KS) distance between the MCMC sample and true distribution amongst all the marginal distributions. This choice reflects the requirements of practical Bayesian statistics, where each parameter will typically have a point estimate and credible region reported, meaning that a supremum distance such as the KS is appropriate in assessing the worst-case accuracy of such figures.

Formally, the Kolmogorov-Smirnov distance for the i -th parameter is defined as

$$D_i = \sup_{x_i} |\tilde{F}_i(x_i) - F_i(x_i)|, \quad i = 1, \dots, d,$$

i.e. the supremum of the absolute value of the difference between the exact CDF F_i and the empirical CDF constructed from the MCMC sample, \tilde{F}_i . The KS distance also has the advantage of being relatively easy to calculate, and it is an integral probability measure with good theoretical properties [Sriperumbudur et al., 2009]. The largest KS distance on the marginal distributions is simply

$$D = \max_{i=1, \dots, d} D_i.$$

Since the empirical CDF is calculated in Monte Carlo, we ran each algorithm 40 times and report the mean and two-sided 95% region of the KS distance in plots such as Figure 4.

As each algorithm that we studied has a different computational cost, in order to maintain a fixed computational budget, each of them must return a sample of different size. In order to meaningfully compare the D statistic across different algorithms, we divided the sample from each algorithm in 40 equal batches. The number was chosen to be 40 as it is large enough to give a detailed account of convergence, but not too large for our computational resources. We then produced the lines in Figure 4 by calculating the D statistic on subsamples formed by an increasing number of batches, with the first value of each line calculated only on one batch, and the last value of each line calculated on the whole sample.

5.1.3 Effects of tolerances

As mentioned above, in most experiments we set both the integration routine absolute tolerance and Brent’s method absolute tolerance to 10^{-10} . We also used the example from Section 5.2.5 to vary these tolerances systematically and assess their impact on accuracy of the posterior samples.

Figure 3 shows how D , the worst Kolmogorov-Smirnov distance on the marginals, increases as we increase ε_{Bre} . In this example, with 8×10^6 samples, the Monte Carlo error dominates for all $\varepsilon_{\text{Bre}} < 10^2$. This result is model dependent, but it supports the point that even though NuZZ uses numerical approximations to sample the switching times, if the numerical error is small, the difference in the posterior is not detectable.

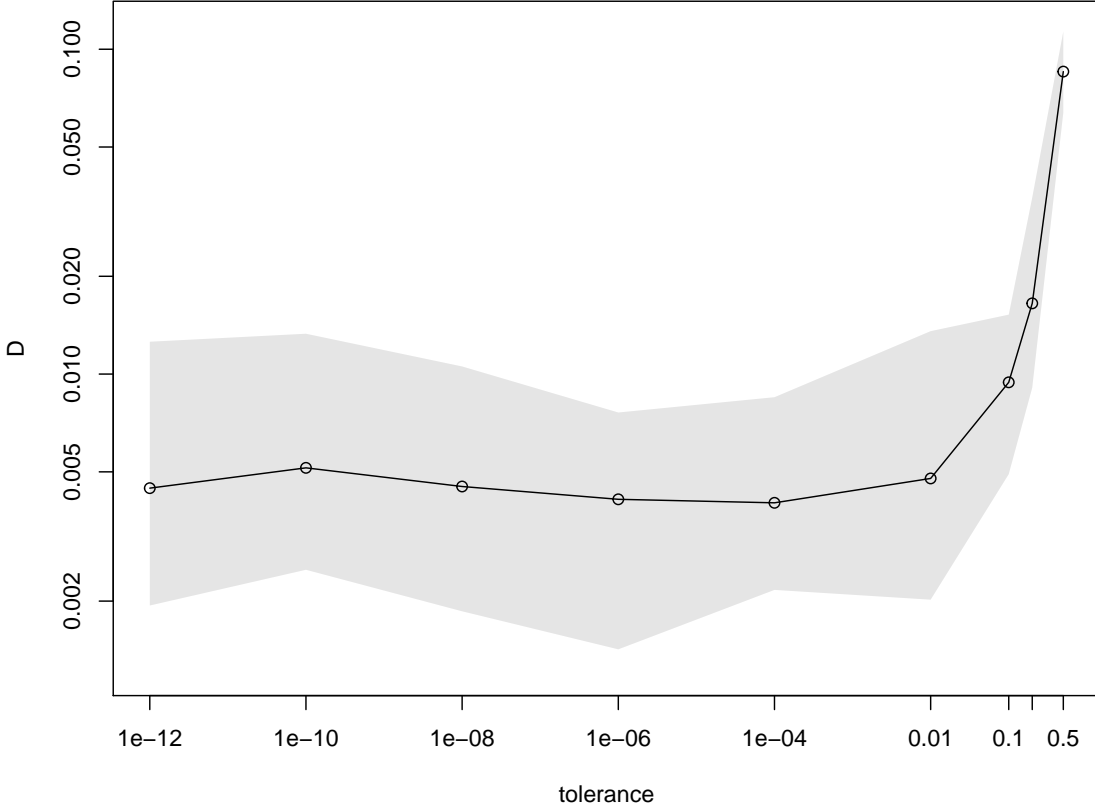


Figure 3: Dependence between the largest Kolmogorov distance on the marginals and the root finding tolerance ε_{Bre} , for a fixed integration tolerance $\varepsilon_{\text{int}} = 10^{-10}$. The computational budget was 6×10^6 epochs, which was processed into 8×10^6 NuZZ samples.

We also tested the influence of the integration error on the quality of the sample from NuZZ, but since the QAGS integration routine performs a minimum of two 21-point Gaussian integration steps, this is often more than enough to reach the condition $\eta_{\text{int}} \leq \varepsilon_{\text{int}} = 10^{-10}$. Therefore we were unable to coarsen this part of the approximation sufficiently in order to produce the analogous plot to Figure 3 for ε_{int} , but simply note that for all the examples we considered, two integration steps are sufficient and the integration tolerance simply acts as a fail-safe for when they are not.

5.1.4 Tuning

One of the many desirable features of ZigZag-like algorithms discussed here is that they only have a handful of parameters to tune. The vector of velocities \mathbf{v}_{init} can affect the mixing of the process. The functions $\gamma_i(\mathbf{x}, \mathbf{v})$ can be set to zero if the target distribution satisfies certain properties [Bierkens et al., 2019], or otherwise they can be made small enough such that they have negligible effects on the dynamics.

The magnitudes of the elements in the vector \mathbf{v} , which do not change from their initial values during

switches, specify the velocity of the process, and their signs correspond to the direction the process is following in each dimension. The sign of one component of the velocity is changed at every iteration, so that the process can properly explore the space. The simplest choice for the initial velocities is $v_i = 1, \forall i = 1, \dots, d$, however it makes sense to have different velocities for components with different scales.

The velocities, like other MCMC parameters, can be tuned adaptively as long as the adaptation satisfies certain conditions [Roberts and Rosenthal, 2007]. When we tune the velocities of the NuZZ algorithm adaptively, we use the history of the process to calculate standard deviations σ_i for each variable on the basis of observed sample properties during the adaptation phase, and normalise them to have fixed speed $\|\mathbf{v}\|_2 = \sqrt{d}$, as the original process. Thus the individual values of the v_i change, but the overall speed of the process remains the same. Explicitly, if we have a set of estimated standard deviations, σ_i , then the velocity update we use is

$$v_i = \frac{\sigma_i}{\|\boldsymbol{\sigma}\|_2} \sqrt{d}. \quad (27)$$

In [Bierkens et al., 2019] the authors give conditions for the ergodicity of the process, and consequently for the functions γ_i . One such condition is that $\gamma_i(\mathbf{x}, \mathbf{v}) = \gamma_i(\mathbf{x}, F_i(\mathbf{v}))$ must be satisfied for the correct density to be targeted. Intuitively speaking, the γ_i functions provide a baseline switching rate and as such make sure that the process does not diverge to infinity. The larger these functions are, however, the more the ZigZag process behaves like a random walk, nullifying the advantages of irreversibility. In the absence of a theoretical result concerning optimal values, we adopt a pragmatic approach based on the heuristic that the γ_i functions should be as small as possible while preserving ergodicity. For simplicity, we let $\gamma_i(\mathbf{x}, \mathbf{v}) = \gamma, \forall i, \mathbf{x}, \mathbf{v}$. If the constant γ is too high, the dynamics will involve unnecessary switches; the algorithm will still be ergodic, but more diffusive, with low values of the switching times τ . We therefore monitor the distribution of τ for each problem, and reduce γ until there is negligible further increase in the τ values. The choice of γ is particularly important for distributions with fat tails, as we will discuss in Section 5.2.5

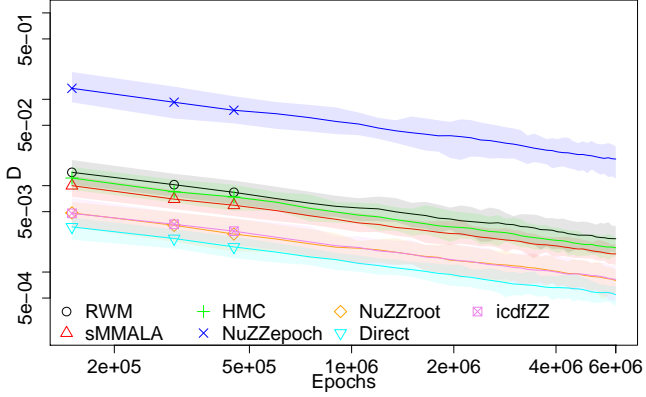
5.2 Description of problems

5.2.1 Standard normal

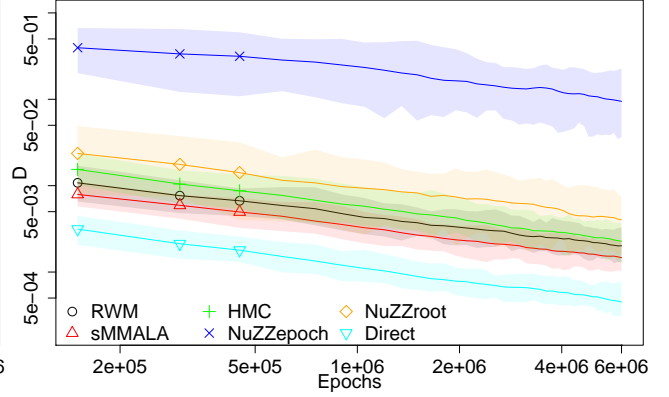
The first model we study is a 10-dimensional standard normal distribution, which lacks any of the challenging features and as such provides a baseline for algorithm performance. It is a model that has analytic solutions for the ZigZag Sampler, so it allows us to compare the performance of the ZigZag with cdf inversion (pink \boxtimes line labelled *icdfZZ* in Figure 4a) with that of the NuZZroot algorithm. As one would expect, direct sampling from the target density shows the fastest convergence.

The three popular algorithms RWM, sMMALA and HMC are all quite close to each other in terms of performance. HMC, which was tuned to take 10 leapfrog steps with step size 0.3 to achieve alternate autocorrelation (identity mass), performs slightly worse than sMMALA. Note that for normal distributions, the Hessian is constant, so there is no difference between sMMALA and standard MALA. The RWM converges quite well, but falls behind sMMALA and HMC in terms of performance.

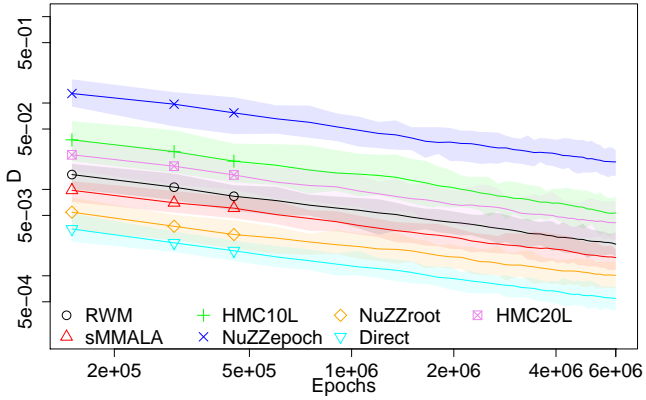
The ZigZag algorithms are represented by the blue \times , yellow \diamond , and pink \boxtimes lines. As expected the NuZZepoch has the slowest convergence, as root finding is expensive in terms of epochs. That leaves the algorithm with a budget of around 8×10^3 switching points, which is not sufficient to explore the density as well as the other algorithms. If this algorithm represents a lower bound for the performance



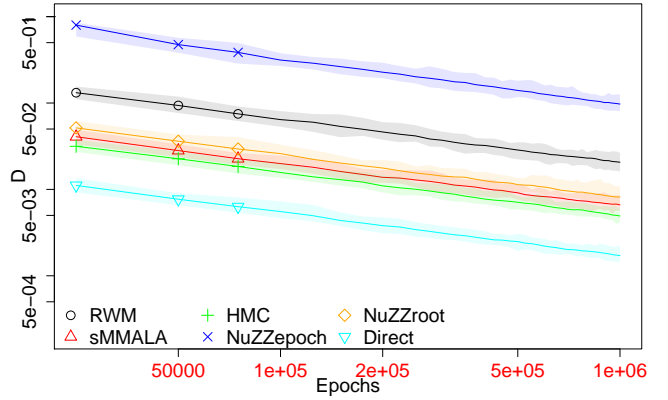
(a) 10-dimensional standard normal.



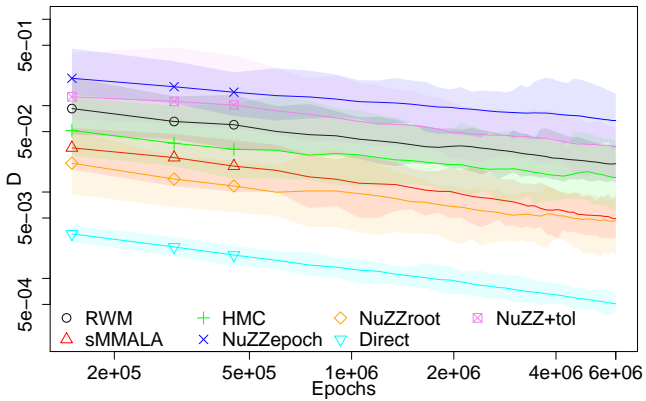
(b) 10-dimensional normal with correlation.



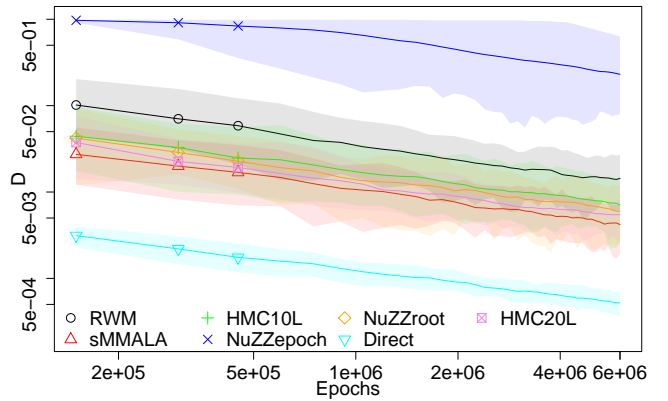
(c) 10-d normal, no correlation and variances $[1^2, 2^2, \dots, 10^2]$.



(d) 100-dimensional standard normal distribution.



(e) 10-dimensional student- t , no correlation, one degree of freedom.



(f) 10-dimensional Hybrid Rosenbrock.

Figure 4: Convergence plots. D represents the Kolmogorov-Smirnov distance between the MCMC sample and the known target.

of ZigZag-like algorithms, the yellow \diamond line of NuZZroot represents the upper bound; its efficiency significantly outperforms every other MCMC algorithm tested.

Of particular interest is the convergence of the analytical version of the ZigZag Sampler (pink \boxtimes line labelled icdfZZ) on this model. The algorithm’s performance is practically indistinguishable from NuZZroot, providing further evidence supporting the discussion of errors in Section 4 above.

5.2.2 Correlation

Having measured the performance of the algorithms on a standard normal, we now proceed to introduce the features of interest which commonly appear in Bayesian inverse problems, starting with correlations. In this section we compare the performance of the algorithms on a 10-dimensional multivariate normal with covariance matrix

$$\Sigma = \begin{bmatrix} 1 & -\alpha & \cdots & \cdots & -\alpha \\ -\alpha & 1 & \alpha & \cdots & \alpha \\ \vdots & \alpha & \ddots & & \vdots \\ \vdots & \vdots & & \ddots & \alpha \\ -\alpha & \alpha & \cdots & \alpha & 1 \end{bmatrix}, \quad (28)$$

where we pick $\alpha = 0.9$. The results can be seen in Figure 4b.

Unsurprisingly, the performance of RWM and sMMALA is quite similar, as they both use rotation matrices to improve their proposals. RWM was tuned to have acceptance rate 25%, with the proposal covariance matrix tuned adaptively on the available MCMC sample. sMMALA was tuned to have 50% acceptance. HMC on the other hand, tuned with step size 0.03 and 10 Leapfrog steps, performs worse than RWM. Tuning the mass matrix does not help mixing in this example. The advantages of following the Hamiltonian path seem to be offset by the high computational cost. The resulting sample is too small to provide a good fit to the target distribution, compared to the other algorithms.

The ZigZag algorithms do not perform well in this setting. The NuZZroot, with velocities tuned adaptively according to the available MCMC sample, performs worse than a well-tuned Random Walk. Hence, ZigZag algorithms may not be a convenient choice if the target model has posteriors that are very strongly correlated. This is largely due to the fact that the process can only travel in certain directions, and if these directions are not conducive with travelling along a ridge in the density, then the process does not mix well. Practically, if the posterior is very close to a multivariate normal then application of an appropriate global transform such as rotation might resolve the problem, but this is a matter for future work.

5.2.3 Different length scales

Another common issue that arises in practice is posteriors whose variables have very different length scales, or variances. Some algorithms, such as HMC, often struggle on these targets, as the length of their trajectory is tuned on one particular scale. Therefore the trajectory will be too long for variables with smaller scales, doubling back and wasting computational resources, while it will be too short for variables with larger scales, giving a more correlated sample.

A common test problem with these features is Neal’s Normal [Neal, 2010], an uncorrelated normal distribution (we take the dimension to be 10, to be consistent with the rest of the test problems) with variances $[1^2, 2^2, \dots, 10^2]$. The results are shown in Figure 4c.

As always, direct sampling is the most efficient method, while NuZZepoch is too expensive to provide a good sample. RWM and sMMALA perform on a similar level, as they apply the same kind of global conditioning to their proposal, which is based on either the available MCMC samples, or the Hessian.

As anticipated, HMC struggles on this target, as the trajectory length can only be tuned optimally on the scale of one variable, while all the other variables will suffer from suboptimal trajectory length. The green line corresponds to HMC tuned as on the other test problems, with step size of 0.3 and 10 leapfrog steps. However, we tried to reduce the number of iterations, to be able to increase the number of leapfrog steps to 20. That version of the HMC algorithm at best marginally improves over its 10-steps counterpart. In both cases, setting the diagonal elements of the mass matrix to the inverse of the standard deviation of the respective marginal distributions does not help mixing, therefore the mass matrix has been taken to be the identity.

The NuZZroot on the other hand, performs well, with the velocities tuned adaptively a total of 10 times during the course of the trajectory. It should be mentioned that the velocity coefficients in each dimension converged to their final value very quickly, making the additional tuning steps redundant. This would suggest that if the target has variables with different scales, ZigZag-like algorithms would perform well.

5.2.4 Large dimension

The next example we study is a standard normal in 100 dimensions. Some algorithms are known to scale particularly poorly with dimension, e.g. RWM, while HMC is better adapted to this scenario. We are not aware of any numerical experiments showing how well the ZigZag dynamics scales with dimension.

For this particular experiment, we reduced the computational budget to 10^6 epochs, to be able to run the repeats in reasonable time. As a consequence, the KS distance is generally one order of magnitude larger than that for the other models. The result of our tests are shown in Figure 4d.

The performance of HMC and sMMALA is quite similar, meaning that the use of gradient information has a positive effect on their performance on this problem. Conversely, the RWM performs significantly worse.

Interestingly, the yellow \diamond line corresponding to the NuZZroot is below the RWM line, suggesting that the benefits of irreversible dynamics outweigh the effectiveness and simplicity of a RWM. However, the yellow \diamond line is above both sMMALA and HMC. Hence gradient and Hessian information help the exploration more than having irreversible dynamics.

5.2.5 Fat tails

In this example we look at how the algorithms perform when the target has fat tails. This feature is particularly common in particle physics, where posteriors are often Cauchy-like, with power-law decay in their tails. The computational budget is reset to 6×10^6 epochs, and the target distribution is a 10-d student- t with one degree of freedom, so that all moments are infinite.

In Figure 4e, the curves are tightly packed with overlapping confidence intervals. RWM, HMC and sMMALA display similar convergence speed, with sMMALA being the fastest. This may be due to the fact that the Hessian is not constant, which may provide some helpful local information to the

dynamics. HMC was tuned to take 10 leapfrog steps, and a step size that left the acceptance ratio at 60-90%. The mass matrix was taken to be the identity matrix. As the moments of the distribution are infinite, it is not possible to tune the proposal variance of the Random Walk adaptively, as it would keep increasing. Therefore we used a fixed identity matrix for the proposal, and we tuned the step size to obtain an acceptance probability of about 25%.

The ZigZag-like algorithms perform quite well. The blue \times line representing the NuZZepoch is not too far from the others. The yellow \diamond line corresponding to the NuZZroot is the second lowest on the chart, outperformed only by direct sampling of the density. The good performance of the ZigZag-like algorithms is due to the fact that the process is more frequently able to make longer excursions into the tails than the other methods, due to the low gradient of the potential in the fat tails.

In this example it was crucial to choose γ such that the exploration is dominated by the irreversible dynamics, as opposed to random switches. Using our pragmatic approach to this problem, as explained in section 5.1.4, after choosing an initial value $\gamma = \gamma_i = 10^{-2}, \forall i = 1, \dots, d$, we run a few test simulations whereby we looked at the maximum switching time value τ_{\max} for each run. As γ decreases, τ_{\max} tends to increase, as the dynamics becomes less diffusive. We noticed that in our example τ_{\max} stopped increasing at around $\gamma = 10^{-4}$, suggesting there would not be any advantage in decreasing γ (and the diffusivity of the process) further.

5.2.6 Position-dependent correlation structure

We move on to study how the algorithms behave in the regime of curved (or non-constant) correlation structure. A distribution belonging to this class cannot be indexed with a global covariance matrix, as global conditioning does not capture the local characteristics of the target. They commonly look like curved ridges, or ‘bananas’, in the state space. These shapes are common in many fields of science, often in hierarchical models or models affected by some sort of degeneracy in their parameter space [House et al., 2016, The Dark Energy Survey Collaboration et al., 2017].

In this section we will use the Hybrid Rosenbrock distribution [Pagani et al., 2019], and more specifically the distribution

$$\pi(\mathbf{x}) = \sqrt{\frac{ab^{d-1}}{\pi^d}} \exp \left\{ -ax_1^2 - b \sum_{i=2}^d (x_i - x_1^2)^2 \right\}, \quad (29)$$

where $\mathbf{x} \in \mathbb{R}^d$, $a = 2.5$, $b = 50$. The parameters a, b have been chosen so that the shape of the distribution does not pose an extreme challenge to the algorithms we are studying. The contours of this distribution generally look like those shown in Figure 2. The results of our experiments are shown in Figure 4f.

It should be noted that the marginals of the Hybrid Rosenbrock are not known analytically, but it is possible to sample from them directly. To produce convergence plots based on the D statistics, we built empirical cumulative distribution functions for each marginal of our target, based on 2×10^{10} samples. The Monte Carlo error introduced in our analysis by this step is therefore negligible.

Even though the curvature is not extreme, the RWM performs significantly worse than the other standard MCMC algorithms. The sMMALA algorithm performs well, as it is designed to deal with this class of densities, and the gap with the other algorithms would be larger if the shape of the target was narrower and with longer tails. HMC works quite well, even though it is difficult to tune for this target. We run two separate versions of HMC, one taking 10 leapfrog steps, and the other taking 20. Both have step size 0.03, identity mass, and a budget of 6×10^6 epochs, which translates into a

sample of 5×10^5 in the first case, and 2.75×10^5 in the second case. The mass matrix was taken to be the identity matrix in both cases. Both versions of HMC perform well, but the HMC version with 20 leapfrog steps appears to perform better, with speed of convergence closer to sMMALA.

The first part of the NuZZepoch has KS distance close to one, which means that the process has not had enough time to escape the local region where it started. However, after $\approx 10^6$ epochs it starts converging like the other algorithms. The yellow \diamond line corresponding to the NuZZroot, is above sMMALA, between the two versions of HMC. This is quite a promising result, as HMC is notoriously difficult to tune, especially on this class of problems, while NuZZ requires little to no tuning at all. The velocity vector was not adapted from the initial values of $\mathbf{v} = (1, \dots, 1)^\top$.

5.2.7 House price data

The last test we perform is on real-world data, specifically on the house-price dataset that we used for our motivating example in Section 1.2 above. As explained in Section 1.2, the target is a normal distribution, $\beta | \{X, \mathbf{y}, \hat{\sigma}\} \sim \mathcal{N}(\hat{\beta}, \hat{\sigma}^2(\mathbf{X}^\top \mathbf{X})^{-1})$. This model has the advantage, therefore, of having known posterior, which allows us to use the same performance metric that we used in the previous tests, and also has an explicit bound for the gradient, which is essential to the ZZCV algorithm.

The House Prices dataset is quite challenging for all the algorithms involved in this test. Its posterior combines multiple features that we previously explored separately. The number of variables is large ($d = 77$), their marginals have very different scales with a difference up to several order of magnitude, and some of the variables are significantly correlated. All of these features commonly occur in real world datasets, which further increases the importance of this test. Due to the challenging nature of this model, the computational budget for this test was increased to 2×10^8 epochs, and the algorithms were started at the Maximum Likelihood Estimate. The results can be seen in Figure 5.

The ZZCV algorithm, represented by the pink \boxtimes line, performs poorly. The very inefficient bound on the gradient and the very high rejection rate on switching points cause the algorithm to spend an inordinate amount of likelihood evaluations to only cover a small distance, resulting in a biased sample.

The green + line representing HMC suggests that the algorithm is converging well, but a much larger number of samples would be needed to give an accurate representation of the posterior.

The HMC algorithm was tuned to take 10^4 leapfrog steps per sample, returning only 2×10^4 samples in total. The step size was fixed to 7×10^{-8} , yielding an acceptance ratio close to 0.6. The reason for such an extreme tuning is that as the variables have very different scales, and the integrator step size needs to be small enough not to diverge when exploring the smallest components, and at the same time the trajectory needs to be long enough that the larger components are explored properly. As our measure of performance is the worst Kolmogorov distance on the marginals, we tune HMC to perform well on the variables with the largest scale, at the expense of wasting computations on the smaller components of the state space. Setting the elements of the mass matrix’s diagonal to the inverse of the standard deviation of the corresponding marginal posterior distribution does not help the exploration of the state space, therefore we took the mass matrix to be the identity.

The HMC performance could be further improved by splitting groups of variables with starkly different scales into separate leapfrog loops. That would allow the larger components to use a larger step size, while the smaller components could reduce the number of leapfrog steps. However, multiple integration loops significantly increase the computational cost, as each gradient evaluation is counted separately.

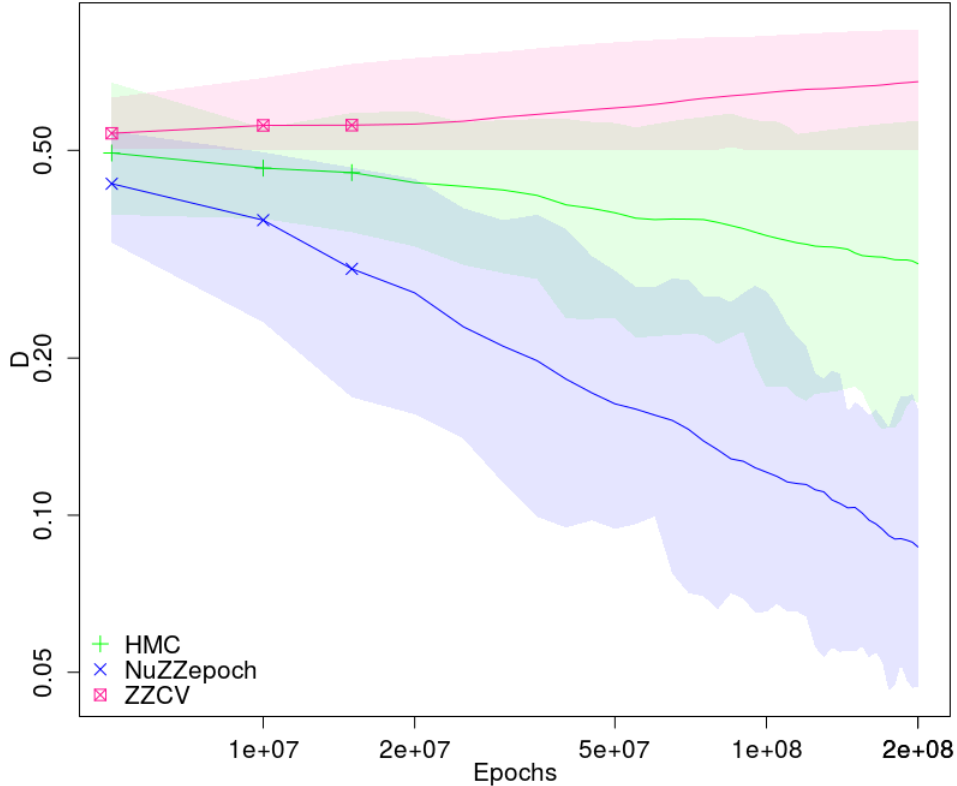


Figure 5: Convergence of the algorithms HMC, ZZCV and NuZZepoch in the Kolmogorov-Smirnov metric on a linear regression model estimated on the House Prices dataset.

Moreover, each loop would have to be tuned separately, making it even harder to tune HMC. Most users use pre-packaged code to run complex algorithms like HMC, and they have no control on the source code. Therefore, we chose not to implement those changes in our test, to further capture the likely performance of the algorithms on real world data.

The blue \times line represent the NuZZ algorithm. On this model, despite its significant computational cost, NuZZ outperforms both ZZCV and HMC by good measure. Furthermore, it requires no bound to function, and does not need to be tuned by the user, as the velocities are adjusted adaptively.

6 Conclusions

In this work we discussed how the standard ZigZag Sampler from [Bierkens et al., 2016] is limited in its applicability to models where an analytical solution is available, or when a bound based on the Jacobian or Hessian is available. We also showed how in practice, some datasets may pose a significant challenge to the ZigZag with control variates algorithm, which may then be outperformed by algorithms with higher asymptotic cost.

We proceeded to present the NuZZ algorithm, which is based on a more efficient implementation of the ZigZag Sampler, and carries out numerically the steps that would otherwise need analytical solutions or efficient bounds. As opposed to the standard ZigZag sampler, NuZZ can now be applied to general models, allowing us to study the properties of the ZigZag dynamics from the practitioner’s point of

view.

Numerical errors in the sampling of the switching times in the NuZZ lead to a perturbation in the invariant distribution of the process. We demonstrated that the Wasserstein distance between the target and the invariant distribution is linearly dependent on the tolerances of both the numerical integration and root finding routines. This demonstrates that the NuZZ can be used to sample from any given target distribution up to a prescribed degree of accuracy.

We tested the ZigZag algorithms against some popular MCMC algorithms, i.e. Random Walk Metropolis, Hamiltonian Monte Carlo and Simplified Manifold MALA, on benchmark problems that display important features that often occur in practice.

Our conclusion is that overall, the ZigZag dynamics is competitive with other popular MCMC dynamics, and in some cases outperforms them even in the absence of super-efficiency through sub-sampling, under the assumption that at most 1 epoch is used per switching event. Notably, when the target has variables with very different scales, or when the target has fat tails, the ZigZag dynamics outperforms all the other algorithms, second only to direct sampling.

Notably, we presented a real life example of an inference problem using house price data with multiple categorical variables, for which NuZZ outperformed ZZCV and HMC, even when taking into account the large number of epochs used in order to find each switching point. Moreover, the NuZZ has significantly fewer parameters to tune than algorithms like HMC, and those that exist can be tuned quite simply, which makes it more robust to misspecification. This demonstrates that NuZZ is not just a tool to enable testing of the ZigZag process’s ability to explore general densities for which bounds on the derivatives of the potential are available, but it is a useful sampling strategy in its own right.

While there are many questions remaining about the ZigZag process and PDMPs in MCMC in general, there are three main directions that naturally lead on from our work. The first is whether the numerical efficiency of NuZZ can be improved, for example by using more tightly integrated, bespoke integration and root-finding routines. The second is whether a more rigorous theoretical understanding of how numerical errors of all kinds propagate through PDMP-based MCMC, which is more complex than for reversible schemes. Finally, the formal definition of the NuZZ through the Sellke construction suggests that other PDMPs based on an interior and active boundary may be amenable to design and analysis.

Acknowledgements

SC and TH are supported by the Alan Turing Institute for Data Science and Artificial Intelligence. TH is additionally supported by the Royal Society. FP would like to thank the Department of Mathematics at the University of Manchester for PhD funding.

References

- [Andrieu et al., 2019] Andrieu, C., Durmus, A., Nsken, N., and Roussel, J. (2019). Hypocoercivity of Piecewise Deterministic Markov Process-Monte Carlo. *arXiv:1808.08592v2*.
- [Bardenet et al., 2017] Bardenet, R., Doucet, A., and Holmes, C. (2017). On Markov Chain Monte Carlo Methods for Tall Data. *J. Mach. Learn. Res.*, 18(1):15151557.
- [Bierkens, 2015] Bierkens, J. (2015). Non-Reversible Metropolis Hastings. *Statistics and Computing (Springer)*, 26:1213 – 1228.
- [Bierkens and Duncan, 2016] Bierkens, J. and Duncan, A. (2016). Limit Theorems for the Zig-Zag Process. *arXiv:1607.08845v1*.
- [Bierkens et al., 2016] Bierkens, J., Fearnhead, P., and Roberts, G. (2016). The Zig-Zag Process and Super Efficient Sampling for Bayesian Analysis of Big Data. *arXiv:1607.03188v1*.
- [Bierkens et al., 2018] Bierkens, J., Kamatani, K., and Roberts, G. (2018). High-dimensional Scaling Limits of Piecewise Deterministic Sampling Algorithms. *arXiv:1807.11358v2*.
- [Bierkens and Roberts, 2016] Bierkens, J. and Roberts, G. (2016). A Piecewise Deterministic Scaling Limit of Lifted Metropolis-Hasting in the Curie-Weiss model. *arXiv:1509.00302v2*.
- [Bierkens et al., 2019] Bierkens, J., Roberts, G., and Zitt, P. (2019). Ergodicity of the ZigZag process. *The Annals of Applied Probability*, 29(4):2266–2301.
- [Bierkens and Verduyn Lunel, 2019] Bierkens, J. and Verduyn Lunel, S. (2019). Spectral Analysis of the ZigZag Process. *arXiv:1905.01691v1*.
- [Bouchard-Côte et al., 2017] Bouchard-Côte, A., Vollmer, S., and Doucet, A. (2017). The Bouncy Particle Sampler: A Non Reversible Rejection-Free Markov Chain Monte Carlo Method. *arXiv:1510.02451v6*.
- [Brooks et al., 2011] Brooks, S., Gelman, A., Jones, G., and Meng, X., editors (2011). *Handbook of Markov Chain Monte Carlo*. Chapman and Hall/CRC, New York.
- [Cotter et al., 2019a] Cotter, C., Cotter, S., and Russell, P. (2019a). Ensemble Transport Adaptive Importance Sampling. *SIAM/ASA Journal on Uncertainty Quantification*, 7(2):444–471.
- [Cotter et al., 2019b] Cotter, S., Kevrekidis, I., and Russell, P. (2019b). Transport Map Accelerated Adaptive Importance Sampling, and Applications to Inverse Problems Arising from Multiscale Stochastic Reaction Networks. *arXiv preprint arXiv:1901.11269*.
- [Cotter et al., 2013] Cotter, S., Roberts, G., Stuart, A., and White, D. (2013). MCMC methods for Functions: Modifying Old Algorithms to Make them Faster. *Statistical Science*, pages 424–446.
- [Davis, 1984] Davis, M. (1984). Piecewise-Deterministic Markov Processes: A General Class of Non-Diffusion Stochastic Models. *Journal of the Royal Statistical Society. Series B (Methodological)*, 46(3):353–388.
- [Davis, 1993] Davis, M. (1993). *Markov Models and Optimization*. Springer.
- [Deligiannidis et al., 2018] Deligiannidis, G., Paulin, D., Bouchard-Côte, A., and Doucet, A. (2018). Randomized Hamiltonian Monte Carlo as Scaling Limit of the Bouncy Particle Sampler and Dimension-Free Convergence Rates. *arXiv:1808.04299v2*.

- [Diaconis et al., 2000] Diaconis, P., Holmes, S., and Neal, R. (2000). Analysis of a Nonreversible Markov Chain Sampler. *Ann. Appl. Probab.*, 10(3):726–752.
- [Duane et al., 1987] Duane, S., Kennedy, A., Pendleton, B., and Roweth, D. (1987). Hybrid Monte Carlo. *Physics Letters B*, 195(2):216–222.
- [Durmus et al., 2019] Durmus, A., Guillin, A., and Monmarch, P. (2019). Geometric Ergodicity of the Bouncy Particle Sampler. *arXiv:1807.05401v2*.
- [Galassi, M., 2017] Galassi, M. (2017). *GNU Scientific Library Reference Manual*. <http://www.gnu.org/software/gsl/>.
- [Gaudreau, 2017] Gaudreau, P. (2017). *House Prices: Dealing with the Missing Data*. <https://www.kaggle.com/clustersrus/house-prices-dealing-with-the-missing-data>.
- [Gillespie, 1977] Gillespie, D. (1977). Exact stochastic simulation of coupled chemical reactions. *The journal of physical chemistry*, 81(25):2340–2361.
- [Girolami et al., 2011] Girolami, M., Calderhead, B., and Chin, S. (2011). Riemann Manifold Langevin and Hamiltonian Monte Carlo Methods. *Journal of the Royal Statistical Society, Series B (Methodological)*.
- [Hastings, 1970] Hastings, W. (1970). Monte Carlo Sampling Methods using Markov Chains and their Applications. *Biometrika*, 57(1):97–109.
- [House et al., 2016] House, T., Ford, A., Lan, S., Bilson, S., Buckingham-Jeffery, E., and Girolami, M. (2016). Bayesian Uncertainty Quantification for Transmissibility of Influenza, Norovirus and Ebola using Information Geometry. *Journal of the Royal Society Interface*, 13(121).
- [Huggins and Zou, 2017] Huggins, J. and Zou, J. (2017). Quantifying the Accuracy of Approximate Diffusions and Markov Chains. *arXiv:1605.06420v4*.
- [Kaggle, 2017] Kaggle (2017). *House Prices: Advanced Regression Techniques*. <https://www.kaggle.com/c/house-prices-advanced-regression-techniques/data>.
- [Kim et al., 1998] Kim, S., Shephard, N., and Chib, S. (1998). Stochastic Volatility: Likelihood Inference and Comparison with ARCH Models. *The Review of Economic Studies*, 65:361–393.
- [Kolesnik and Ratanov, 2013] Kolesnik, A. and Ratanov, N. (2013). *Telegraph Processes and Option Pricing*. Springer.
- [Löpker and Palmowski, 2013] Löpker, A. and Palmowski, Z. (2013). On Time Reversal of Piecewise Deterministic Markov Processes. *Electronic Journal of Probability*, 18(13):129.
- [Ma et al., 2016] Ma, Y., Fox, E., Chen, T., and Wu, L. (2016). A Unifying Framework for Devising Efficient and Irreversible MCMC Samplers. *arXiv:1608.05973v3*.
- [Metropolis et al., 1953] Metropolis, N., Rosenbluth, A., Rosenbluth, M., Teller, A., and Teller, E. (1953). Equation of State Calculations by Fast Computing Machines. *The Journal of Chemical Physics*, 21(6):1087–1092.
- [Neal, 2010] Neal, R. (2010). MCMC using Hamiltonian dynamics. *Handbook of Markov Chain Monte Carlo*, 54:113–162.
- [Ottobre, 2016] Ottobre, M. (2016). Markov Chain Monte Carlo and Irreversibility. *Reports on Mathematical Physics*, 77(3):267 – 292.

- [Pagani et al., 2019] Pagani, F., Wiegand, M., and Nadarajah, S. (2019). An n-dimensional Rosenbrock Distribution for MCMC Testing. *arXiv:1903.09556*.
- [Peters and de With, 2012] Peters, E. and de With, G. (2012). Rejection-Free Monte Carlo Sampling for General Potentials. *Physical Review E*, 85:026703+.
- [Press et al., 2007] Press, W., Teukolsky, S., Vetterling, W., and Flannery, B. (2007). *Numerical Recipes 3rd Edition: The Art of Scientific Computing*. Cambridge University Press, New York, NY, USA, 3 edition.
- [Rapaport, 2009] Rapaport, D. (2009). The Event-Driven Approach to N-Body Simulation. *Progress of Theoretical Physics Supplement*, N/A(178):5 – 14.
- [Robert and Casella, 2011] Robert, C. and Casella, G. (2011). A Short History of Markov Chain Monte Carlo: Subjective Recollections from Incomplete Data. *Statist. Sci.*, 26(1):102–115.
- [Roberts and Rosenthal, 1997] Roberts, G. and Rosenthal, J. (1997). Optimal Scaling of Discrete Approximations to Langevin Diffusions. *J. R. Statist. Soc. B*, 60:255–268.
- [Roberts and Rosenthal, 2007] Roberts, G. and Rosenthal, J. (2007). Coupling and Ergodicity of Adaptive Markov Chain Monte Carlo Algorithms. *Journal of applied probability*, 44(2):458–475.
- [Ross, 2011] Ross, N. (2011). Fundamentals of Steins method. *Probab. Surveys*, 8:210–293.
- [Sellke, 1983] Sellke, T. (1983). On the Asymptotic Distribution of the Size of a Stochastic Epidemic. *Journal of Applied Probability*, 20(2):390394.
- [Sriperumbudur et al., 2009] Sriperumbudur, B., Fukumizu, K., Gretton, A., Schlkopf, B., and Lanckriet, G. (2009). On Integral Probability Metrics, ϕ -divergences and Binary Classification. *arXiv:0901.2698v4*.
- [The Dark Energy Survey Collaboration et al., 2017] The Dark Energy Survey Collaboration et al. (2017). Cosmology from Cosmic Shear with DES Science Verification Data. *arXiv*.
- [Turitsyn et al., 2011] Turitsyn, K., Chertkov, M., and Vucelja, M. (2011). Irreversible Monte Carlo Algorithms for Efficient Sampling. *Physica D: Nonlinear Phenomena*, 240(4):410 – 414.
- [Vanetti et al., 2018] Vanetti, P., Bouchard-Côte, A., Deligiannidis, G., and Doucet, A. (2018). Piecewise-Deterministic Markov Chain Monte Carlo. *arXiv:1707.05296v2*.
- [Wu and Robert, 2017] Wu, C. and Robert, C. (2017). Generalized Bouncy Particle Sampler. *arXiv:1706.04781v2*.
- [Zhao and Bouchard-Côte, 2019] Zhao, T. and Bouchard-Côte, A. (2019). Analysis of high-dimensional Continuous Time Markov Chains using the Local Bouncy Particle Sampler. *arXiv:1905.13120v3*.

A Details of Proof of Theorem 2

Our starting point is Equation (16) above, which we will re-write as:

$$\begin{aligned}
 & \underbrace{\int_{\mathcal{X}} \sum_{v \in \mathcal{V}} \int_{\mathcal{Q}_0} v \frac{\partial f}{\partial x} \Big|_{(x,v,q)} e^{-U(x)-q} dq dx}_{\text{First term, } I_1} - \underbrace{\int_{\mathcal{X}} \sum_{v \in \mathcal{V}} \int_{\mathcal{Q}_0} \Lambda(x, v) \frac{\partial f}{\partial q} \Big|_{(x,v,q)} e^{-U(x)-q} dq dx}_{\text{Second term, } I_2} + \\
 & \underbrace{\int_{\mathcal{X}} \sum_{v \in \mathcal{V}} \left(\int_{\mathcal{Q}_0} f(x, -v, q) e^{-q} dq - f(x, v, 0) \right) \Lambda(x, v) e^{-U(x)} dx}_{\text{Third term, } I_3} = 0. \quad (30)
 \end{aligned}$$

To verify this equation, we proceed by analysing each of the three terms individually. We will often exchange the order of integration in integrals, making use of the Fubini-Tonelli theorem. Rearranging the factors and applying integration by parts, the first term becomes

$$\begin{aligned}
 I_1 &= \int_{\mathcal{X}} \sum_{v \in \mathcal{V}} \int_{\mathcal{Q}_0} v \frac{\partial f}{\partial x} \Big|_{(x,v,q)} e^{-U(x)-q} dq dx \\
 &= \sum_{v \in \mathcal{V}} \int_{\mathcal{Q}_0} v e^{-q} \int_{\mathcal{X}} \frac{\partial f}{\partial x} \Big|_{(x,v,q)} e^{-U(x)} dx dq \\
 &= \sum_{v \in \mathcal{V}} \int_{\mathcal{Q}_0} v e^{-q} \left([f(x, v, q) e^{-U(x)}]_{x=-\infty}^{\infty} + \int_{\mathcal{X}} f(x, v, q) \frac{dU}{dx} e^{-U(x)} dx \right) dq \\
 &= \int_{\mathcal{X}} \sum_{v \in \mathcal{V}} \int_{\mathcal{Q}_0} v f(x, v, q) \frac{dU}{dx} e^{-U(x)-q} dq dx,
 \end{aligned} \quad (31)$$

where the term in square brackets on the third line is zero as we work with target densities $\pi(x) \propto e^{-U(x)}$ that tend to zero as $x \rightarrow \pm\infty$. Again, we rearrange the factors and apply integration by parts to the second term:

$$\begin{aligned}
 I_2 &= \int_{\mathcal{X}} \sum_{v \in \mathcal{V}} \int_{\mathcal{Q}_0} \Lambda(x, v) \frac{\partial f}{\partial q} \Big|_{(x,v,q)} e^{-U(x)-q} dq dx \\
 &= \int_{\mathcal{X}} \sum_{v \in \mathcal{V}} \Lambda(x, v) e^{-U(x)} \int_{\mathcal{Q}_0} \frac{\partial f}{\partial q} \Big|_{(x,v,q)} e^{-q} dq dx \\
 &= \int_{\mathcal{X}} \sum_{v \in \mathcal{V}} \Lambda(x, v) e^{-U(x)} \left([f(x, v, q) e^{-q}]_{q=0}^{\infty} - \int_{\mathcal{Q}_0} f(x, v, q) \frac{de^{-q}}{dq} dq \right) dx \\
 &= \int_{\mathcal{X}} \sum_{v \in \mathcal{V}} \int_{\mathcal{Q}_0} \Lambda(x, v) f(x, v, q) e^{-U(x)-q} dq dx - \int_{\mathcal{X}} \sum_{v \in \mathcal{V}} \Lambda(x, v) f(x, v, 0) e^{-U(x)} dx.
 \end{aligned} \quad (32)$$

Finally, the third term reduces to

$$\begin{aligned}
 I_3 &= \int_{\mathcal{X}} \sum_{v \in \mathcal{V}} \left(\int_{\mathcal{Q}_0} f(x, -v, q) e^{-q} dq - f(x, v, 0) \right) \Lambda(x, v) e^{-U(x)} dx \\
 &= \int_{\mathcal{X}} \sum_{v \in \mathcal{V}} \int_{\mathcal{Q}_0} f(x, -v, q) e^{-q} \Lambda(x, v) e^{-U(x)} dq dx - \int_{\mathcal{X}} \sum_{v \in \mathcal{V}} f(x, v, 0) \Lambda(x, v) e^{-U(x)} dx \\
 &= \int_{\mathcal{X}} \sum_{v \in \mathcal{V}} \int_{\mathcal{Q}_0} \Lambda(x, -v) f(x, v, q) e^{-U(x)-q} dq dx - \int_{\mathcal{X}} \sum_{v \in \mathcal{V}} \Lambda(x, v) f(x, v, 0) e^{-U(x)} dx.
 \end{aligned} \quad (33)$$

Substituting (31), (32) and (33) into (30), we obtain

$$I_1 - I_2 + I_3 = \int_{\mathcal{X}} \sum_{v \in \mathcal{V}} \int_{\mathcal{Q}_0} \left(v \frac{dU}{dx} - (\Lambda(x, v) - \Lambda(x, -v)) \right) f(x, v, 0) e^{-U(x)-q} dq dx = 0, \quad (34)$$

which will hold if

$$v \frac{dU}{dx} = \Lambda(x, v) - \Lambda(x, -v). \quad (35)$$

Then from (3), we have

$$\Lambda(x, v) = \left(0 \vee v \frac{dU}{dx} \right) + \gamma(x, v). \quad (36)$$

Substituting (36) into (35), we see that (35) is satisfied and hence (34) is satisfied, meaning that we have demonstrated Equation (16) as required.